Int J Adv Manuf Technol (2016) 86:2301–2308
DOI 10.1007/s00170-016-8381-2

ORIGINAL ARTICLE

Investigation on droplet momentum in VPPA-GMAW hybrid welding of aluminum alloys

Haitao Hong[1] · Yongquan Han[1] · Maohua Du[1] · Jiahui Tong[1]

Received: 11 June 2015 / Accepted: 13 January 2016 / Published online: 25 January 2016

Abstract Variable polarity plasma arc-gas metal arc welding (VPPA-GMAW) is a superior technology for welding thick plates of high-strength aluminum alloys. It integrates the advantages of energy focusing and high penetration depth in VPPA welding, and those of high welding efficiency and wide range of technological parameters in GMAW process. In this work, we investigated the droplet momentum in paraxial VPPA-GMAW hybrid welding of 7A52 aluminum alloys, and the technological parameters of welding process was also optimized. The images of droplet transfer were captured by high-speed camera, while the droplet speeds and sizes were statistically analyzed by *t* tests of independent samples. The results showed that the speeds of droplet arriving at the weld pool were significantly between GMAW and VPPA-GMAW processes, and the droplet speed increases with increasing plasma currents within a certain range. Meanwhile, the droplet momentum in VPPA-GMAW process is larger than that in conventional GMAW process. We also found that as the droplet momentum increased, the depression of weld pool grew more obvious and greatly facilitated the deep-penetration welding. In VPPA-GMAW process, it became more and more easier for the droplet to fall off the wire when the electromagnetic force gradually increased during pulse period. Droplet movement through the arc zone was further accelerated since the central pressure of arc column increased during base period. This research can provide some theoretical support for thick plate welding of high-strength aluminum alloys and help for deeper understanding of the hybrid arc coupling mechanism.

Keywords Variable polarity plasma arc-gas metal arc welding · Droplet momentum · Droplet transfer · *T* test · Aluminum alloys

1 Introduction

Owing to their high specific strength and high corrosion resistance, aluminum alloys have been widely applicated in many fields like aerospace, automobile, pressure vessel, etc. Among various welding processes of aluminum alloys, pulse gas metal arc welding (GMAW) shows a great advantage due to its ease of automation and high production efficiency [1, 2]. However, the introduction of thick-plate aluminum alloys welded structures brought challenges to GMAW process. Excessive welding current in GMAW process not only breaks the stability of droplet transfer and weld pool but also leads to the formation of coarse grain. Moreover, the strengthening precipitates are coarsened or dissolved due to the local thermal cycle for heat-treatable aluminum alloys. This would seriously reduced the mechanical properties of the welded joint [3, 4].

In order to overcome the above-mentioned problem, plasma-GMAW process was developed. In 1972, Essers et al. [5] in Philips Research Laboratories firstly introduced the coaxial plasma-GMAW process. The GMAW arc, droplet, and wire tip are all immersed in plasma arc. Plasma-GMAW process shows advantages in improving the welding efficiency and reducing welding spatter [6–8]. A great many investigations on droplet transfer of coaxial plasma-GMAW process have been reported. Among them, Hertel et al. [9] established numerical models of plasma-GMAW arc,

✉ Yongquan Han
nmhyq@sina.com

[1] Key Laboratory of Material Forming, Inner Mongolia University of Technology, Hohhot 010051, China

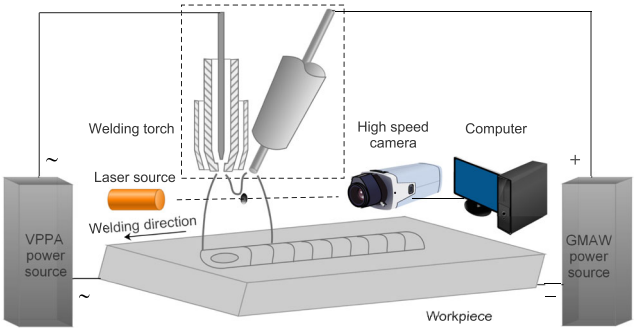

Fig. 1 Experimental setup including data acquisition system for VPPA-GMAW welding

droplet detachment and weld pool. Bai et al. [10, 11] investigated the droplet transition modes. However, there are still some serious problems for plasma-GMAW process to overcome in order to weld thick-plate aluminum alloys. Firstly, because of the unique structure of coaxial welding torch, the plasma power is only able to work on low current ranges. The electrode of GMAW process always keeps positive in order to obtain stable spray transfer. To avoid series arc phenomenon, the tungsten electrode also keeps positive. High working currents for thick-plate welding are limited due to the serious tungsten electrode loss. Secondly, since the GMAW contact tube stays inside plasma constricting nozzle, the plasma arc is not so concentrated. Thirdly, copper or carbon ring electrodes are employed in coaxial welding torch, which shows relatively poorer electron emission ability and further reduces the current density of plasma arc. Last but not least, the coupling effects between plasma and GMAW arc greatly influence the droplet transfer stability. By now, there are many previous reports on the above-mentioned problems. Ton [12] demonstrated that part of GMAW current flows toward the outer region of the plasma arc zone through optical spectroscopy analysis. Terasaki et al. [13] proposed that plasma arc was not only able to heat the welding wire but also change the current channel and the stress state of welding droplet. Essers et al. [14] found that arc around the tip of welding wire tended to rotate at high currents, which made droplet transfer to the pool less concentrated. Resende et al. [15] studied the relationship between plasma current and geometric dimensioning of bead weld. They claimed that GMAW arc is less concentrated, which leads to lower droplet speed. Arc divergence resulted in reduced speed of droplet arriving at weld pool, therefore penetration depth was reduced as plasma current increased.

VPPA-GMAW integrates the advantages of energy focusing and high penetration depth in VPPA welding [16–20], and those of high welding efficiency and wide range of technological parameters in GMAW process. It has been successfully used to various areas, like the wind turbine generator tower, oil pipeline, mobile covering, etc. VPPA-GMAW process is able to reduce the heat input and welding deformation. It also has cathode cleaning ability, thus being especially appropriate to weld aluminum alloys. In VPPA-GMAW process, paraxial welding torch has been used. In comparison with coaxial plasma-GMAW, it shows a smaller constricting nozzle, thus enabling acquirement of concentrated plasma arc. As the electrode distance increases, the interactions between VPPA and GMAW arc are smaller and smaller. Thus the droplet transfer is much more stable, facilitating the deep-penetration welding.

In this research, the momentum of droplet arriving at the weld pool was evaluated to analyze the droplet transfer characteristics in VPPA-GMAW process, and the welding process was optimized for 7A52 aluminum alloys with thickness of 10 mm.

2 Experimental

VPPA-GMAW hybrid welding system consists of VPPA welding power supply (Fronius MagicWave3000), GMAW power supply (Fronius TPS4000), SUPER-MIG welding torch, and KUKA robot. The experimental setup including data acquisition system is schematically illustrated in Fig. 1.

SUPER-MIG welding torch includes a plasma torch perpendicular to working plane and a GMAW torch at an angle of 16° with the plasma torch. The distance between plasma and GMAW torch keeps 8 mm, and the distance from the nozzle to workpiece keeps 10 mm.

Bead weld with various parameters was performed on the flat position by VPPA-GMAW process. 7A52 aluminum alloys with thickness of 10 mm and ER5183 with diameter of 1.6 mm were employed as base metal and welding wire respectively, whose chemical compositions were shown in Table 1. Thoriated tungsten electrode with diameter of 3.2 mm was used. Orifice gas and GMAW shielding gas

Table 1 Chemical compositions of base metal and welding wire (percent by weight)

	Zn	Mg	Cu	Mn	Cr	Ti	Zr	Fe	Si	Al
7A52	4.3	2.1	0.06	0.24	0.16	0.09	0.09	0.3	0.25	Remainder
ER5183	0.25	4.95	0.01	0.75	0.12	0.15	–	0.4	0.4	Remainder

Table 2 Welding parameters (DCEN represents direct current electrode negative, and DCEP represents direct current electrode positive)

Experiment No.	I_{DCEN} (I/A)	I_{DCEP} (I/A)	t_{DCEN} (t/ms)	t_{DCEP} (t/ms)	f_{VPPA} (f/Hz)	I_{GMAW} (I/A)	U_{GMAW} (U/V)
1	0	0	0	0	0	200	20.0
2	90	126	20	4	42	200	20.0
3	120	168	20	4	42	200	20.0
4	160	224	20	4	42	200	20.0
5	120	168	10	2	84	200	20.0
6	120	168	5	1	126	200	20.0
7	120	168	2.5	0.5	168	200	20.0
8	130	182	20	4	42	320	23.5

were surrounded by the overall shielding gas. High-purity argon was used in three gases with gas flow rates of 3.5, 23, and 40 L·min^{-1}, respectively. The welding speed was controlled to be 800 mm·min^{-1}. And welding parameters were shown in Table 2. A high-speed camera of Red Lake Y4 was used to capture the images of droplet transfer based on the principle of optical polarization [21]. To protect the CCD sensor of camera from damage by strong arc light, neutral density filters (ND 4 and ND 8) were mounted in front of camera lens. Laser source with a narrow-band optical filter (808 ± 5 nm) was used as backlight to decrease the effect of welding arc. The sample frequency for capturing droplet transfer images was 3500 frames·s^{-1} with exposure time of 10 μs.

The captured droplet transfer images were imported into motion analysis module of IDT Motion Studio, a bundled software of high-speed camera. Droplet speeds and sizes were obtained precisely by defining feature points of images.

The overall data of droplet speeds and sizes were statistically analyzed by independent samples t test to know whether there was significant difference between GMAW and VPPA-GMAW processes. The parameters were considered to be significantly different when t test value was less than 0.05. The t tests were performed using R software (version 3.2.0).

3 Results and discussion

3.1 Droplet transfer characteristics

The numbered images in Fig. 2 show the droplet transfer behavior of GMAW and VPPA-GMAW processes in one period. It can be observed from the images that the droplet transfer modes are both projected transfer in two processes and their droplet sizes are approximately the same. The influence of plasma arc on GMAW arc is shown in Fig. 3. Due to the existence of plasma arc, the anode area of GMAW arc increases relatively during pulse period. And during base period, GMAW arc becomes relatively contractive.

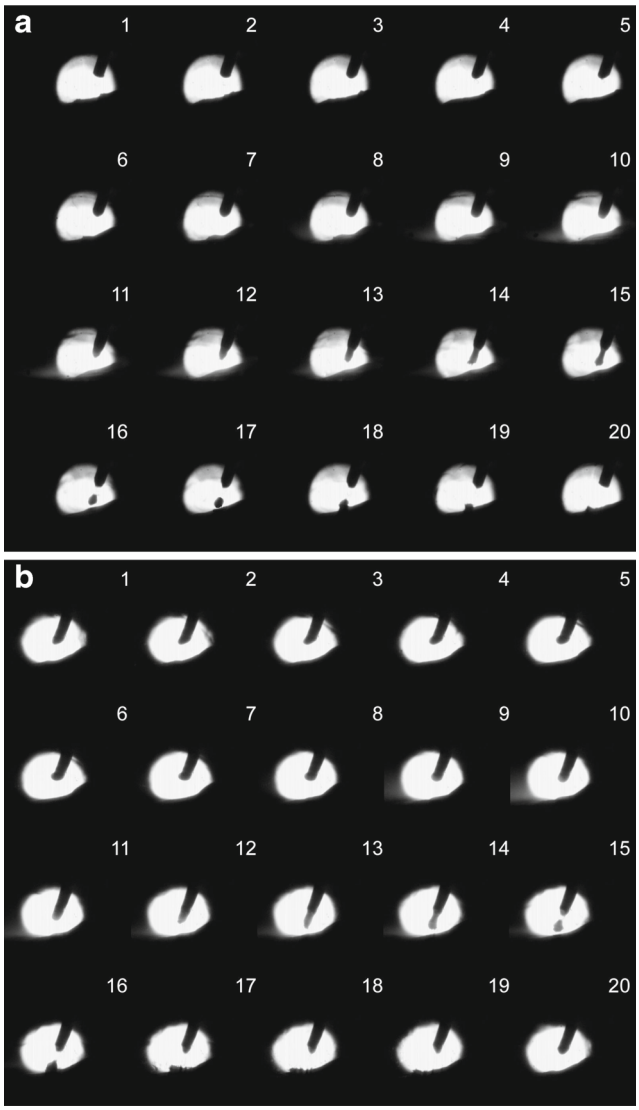

Fig. 2 The high-speed images of droplet transfer in one period. **a** GMAW process in experiment 1. **b** VPPA-GMAW process in experiment 4

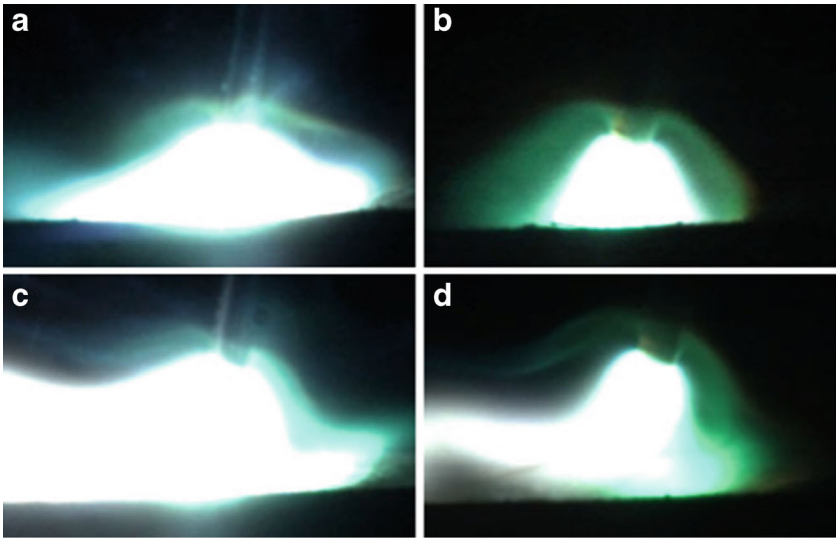

Fig. 3 GMAW arc shape. **a** GMAW process during pulse period. **b** GMAW process during base period. **c** VPPA-GMAW process during pulse period. **d** VPPA-GMAW process during base period

Nine random periods of droplet transfer were chosen as research objects in each experiment. Droplet speeds and sizes were obtained precisely by motion analysis module of IDT Motion Studio software, and the results are shown in Fig. 4. We can observe that droplet speeds tend to increase with increasing plasma current in a certain range. However, excessive plasma current reduces the stability of droplet transfer and welding pool, leading to the formation of the weld seam wrinkle.

Droplet swings with VPPA welding current direction periodically changes. The trajectory of droplet movement cannot be affected significantly by limited swing in a certain frequency range. However, droplet falls off the end of wire with irregular shape due to intense swing when frequency further increase. The effect of the frequency of VPPA on droplet transfer is shown in Fig. 5. The orientation of droplet movement becomes more uncertain, and it is not beneficial for droplet to achieve stability.

It is a complicated physicochemical process with coupling effects of thermal, electric, and mechanical field for droplet falling off welding wire. Due to the existence of a great deal of random interference, droplet speeds are distributed in a limited region. Therefore, statistical analyses of droplet transfer are required before quantitative analysis.

3.2 Statistical analyses

Independent sample t tests were performed for statistical analysis of droplet speeds and sizes of GMAW and VPPA-GMAW processes. Null hypothesis is defined as that there is no significant difference, and alternative hypothesis is defined as the opposite. For two-side hypothesis test, the problem can be formulated as follows:

$$H_0 : v_i = v_j, H_1 : v_i \neq v_j \tag{1}$$

$$H_0 : r_i = r_j, H_1 : r_i \neq r_j \tag{2}$$

where H_0 is null hypothesis, H_1 is alternative hypothesis, v_i and v_j are the droplet speeds in GMAW and VPPA-GMAW processes, respectively. r_i and r_j are the droplet radius. To ensure that testing samples are random samples from normal population, Shapiro-Wilk's and Bartlett's methods were separately used to test normality and variance homogeneity of the data. Hommel's multiple comparison method is used to modified p values. Results of independent sample t tests on droplet speeds and sizes are summarized and presented in Table 3. We can observe that all date meet the requirements

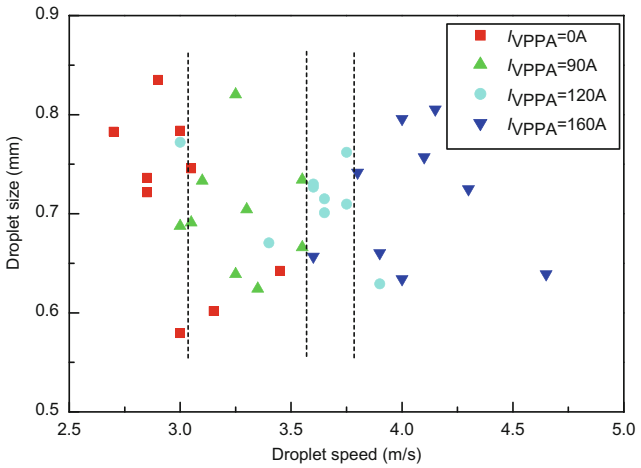

Fig. 4 Droplet size vs. speed arriving at the pool in experiment 1–4

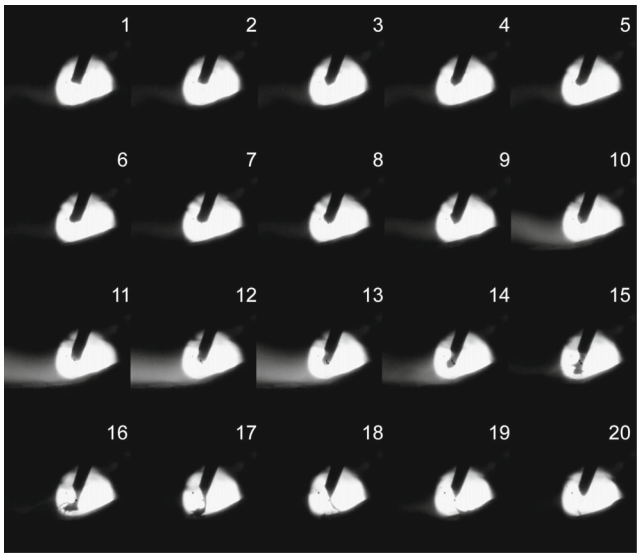

Fig. 5 The high-speed images of droplet transfer in one period with VPPA frequency of 168 Hz

of normality and variance homogeneity. With a common statistical significance defined as $p < 0.05$ for all stages, the difference in droplet speeds is statistically significant, while that of droplet sizes is not. And the droplet arriving at the weld pool in VPPA-GMAW process shows a higher speed than that in GMAW process.

3.3 Droplet momentum

With welding torch moving, the droplet impacts on different area. Meanwhile, droplets transfer into the pool over a period of time. The droplet momentum can be calculated through the following formula [22]:

$$M = \frac{\rho \pi d^3 v_d f}{6 v_{\mathrm{TS}}} \tag{3}$$

Where ρ is droplet density (kg·m^{-3}), d is droplet diameter (m), v_d is droplet speed arriving at weld pool (m·s^{-1}), f is droplet transfer frequency (Hz), and v_{TS} is travel speed (m·s^{-1}). Figure 6 shows the average values of droplet momentum and some related parameters.

The results show that droplet momentum increases with increasing plasma current. The droplet creates pits on the weld pool surface, and the pits would not disappear until the next droplet impact. The droplets constantly fall into the same pit so that the heat in the overheated droplet efficiently transfers to the pool bottom. The depression of weld pool grows more and more obvious with increasing droplet momentum, thus greatly facilitating the deep-penetration welding. Figure 7 presents cross sections of bead weld in GMAW and VPPA-GMAW processes. In Fig. 7a, b, the depth of penetration effectively increases in VPPA-GMAW process. The cross sections with various VPPA frequency parameters are shown in Fig. 7b–d. The result shows that the penetration depth are approximately the same, thus the frequency of VPPA (42–126 Hz) has little effect on droplet speed.

3.4 Droplet acceleration mechanism

The movement of droplet arriving at weld pool is composed of two parts: detaching from the end of wire and moving toward weld pool through the arc zone. The process of droplet transfer is schematically shown in Fig. 8. According to the theory of static force balance, the main forces on droplet include gravity, electromagnetic force, plasma drag force, and surface tension when it detaches from the end of wire. Waszink et al. [23] verified that the influence of gravity and plasma drag force on droplet is relatively smaller. Surface tension depends wire radius and surface tension coefficient, whose values are the same in two processes. Therefore, the electromagnetic force is the dominant force

Table 3 Results of independent sample t tests on droplet speeds and sizes

Variable	Unit	Mean	SD	Shapiro-Wilk's test	Bartlett's test	p_{ij}^a			
v_1	m/s	2.994	0.216	0.468	0.655	1	0.026	5.9E-05	1.3E-09
v_2	m/s	3.267	0.198	0.448		0.026	1	0.019	5.9E-07
v_3	m/s	3.589	0.259	0.079		5.9E-05	0.019	1	0.001
v_4	m/s	4.056	0.302	0.883		1.3E-09	5.9E-07	0.001	1
r_1	mm	0.714	0.088	0.496	0.297	1	0.99	0.99	0.99
r_2	mm	0.701	0.059	0.589		0.99	1	0.99	0.99
r_3	mm	0.713	0.044	0.752		0.99	0.99	1	0.99
r_4	mm	0.713	0.067	0.222		0.99	0.99	0.99	1

A p_{ij} represents multiple comparison value of experiment i to experiment j

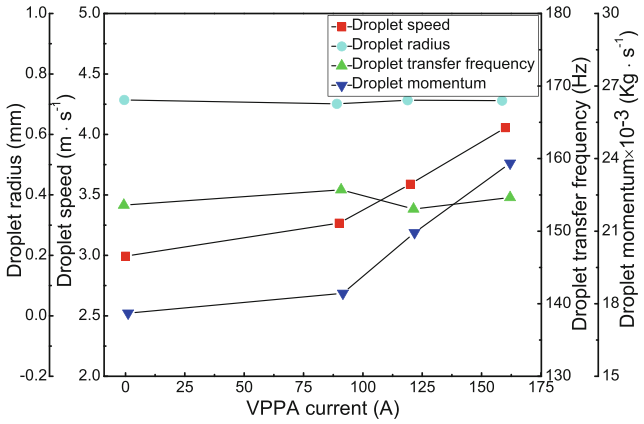

Fig. 6 Average values of droplet momentum and some related parameters with GMAW current of 200 A

facilitating droplet transfer, and it can be evaluated by the formula [23]:

$$F_{em} = \frac{\mu_0 I^2}{4\pi}\left(\frac{1}{2} + ln\frac{r_a}{r_w}\right) \tag{4}$$

Where μ_0 is the magnetic permeability of vacuum, I is welding current (A), r_a is the radius of arc at anode (m), and r_w is the radius of welding wire (m). r_a is determined by thermal ionization degree of arc, which decreases with higher temperature. During pulse period of GMAW process, GMAW arc size is increased, therefore the overlapping region of VPPA and GMAW arc grows larger. Due to the heat transferred from plasma arc, the surrounding temperature of GMAW arc column increases, leading to reduced thermal ionization degree and increased r_a value. Therefore, higher initial speed can be achieved with larger electromagnetic force in VPPA-GMAW process. As VPPA welding current increases, arc size and overlapping region grow larger, resulting in stronger electromagnetic force acting on droplet. Thus, droplet speed increases with increasing plasma current in a certain range.

Since arc expands from the welding wire to workpiece, the current densities vary in different positions among them. For example, the current density in position M is larger than that in position N. Therefore, the droplet is accelerated by pressure from the electromagnetically induced flow through the arc zone [24]. Arc pressure can be calculated by the formula [25]:

$$P_r = \int_R^r dPr = \frac{I^2}{\pi R^4}(R^2 - r^2) \tag{5}$$

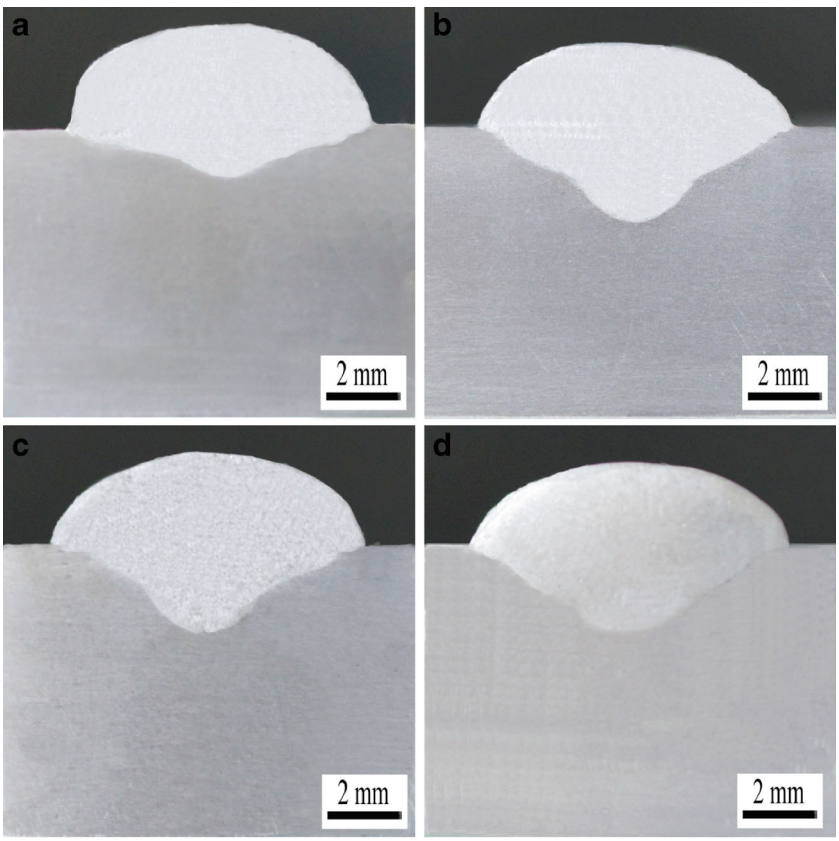

Fig. 7 Cross sections of bead weld tests. **a** GMAW process in experiment 1. **b** VPPA-GMAW process in experiment 3. **c** VPPA-GMAW process in experiment 5. **d** VPPA-GMAW process in experiment 6

Where R is the radius of GMAW arc column (m), and r is the distance from any point to the center of the arc column (m). If droplet moves along the axis of welding wire, namely $r = 0$, arc pressure acting on droplet surface can be expressed as:

$$F = \pi r_d^2 \cdot P_0 = r_d^2 \cdot \frac{I^2}{R^2} \tag{6}$$

Where r_d is the radius of droplet (m). The stiffness of GMAW arc decreases during base period of GMAW process, therefore it would be easily affected by external force. Radial component of the additional electromagnetic force from VPPA can constrict GMAW arc. Hence pressure in the center of arc column increases with decreasing cross-section area of arc. Since the droplet sizes are approximately the same in two processes, the force acting on droplet surface in VPPA-GMAW process is stronger than that in GMAW process. As a consequence, the droplet speed further increases through arc zone during base period.

The frequency variation of VPPA can only affect the duration of DCEN and DCEP, but little to the amplitude of welding current. When frequency varies, arc size remains unchanged, thus droplet speed is also not affected. However, the frequency variation would greatly affect the stability of welding process. If the frequency is too low, tungsten electrode loss can be serious when DCEP time is long enough. Besides, GMAW arc swings periodically as the current direction of VPPA welding changes. Although the amplitude of arc swing can be reduced by applying external transverse alternative magnetic field at nozzle, droplet oscillates vigorously on wire tip with frequency further increased. The stability of droplet transfer is severely disrupted, thus unfavorable for deep-penetration welding.

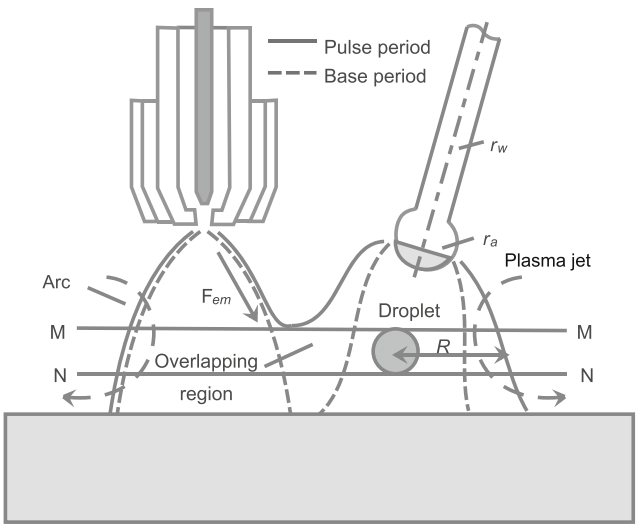

Fig. 8 Schematic illustration of droplet transfer in VPPA-GMAW process

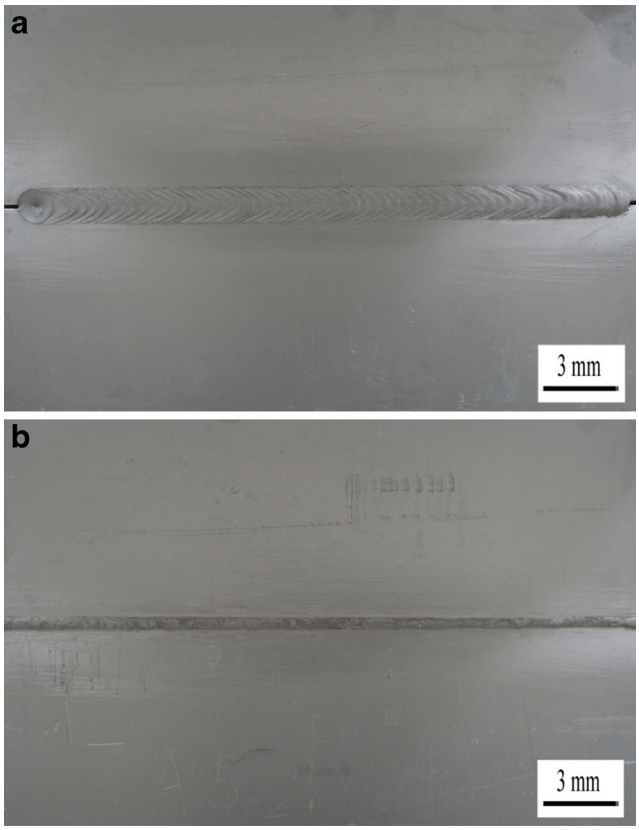

Fig. 9 Images of the weld seam. **a** front side. **b** back side

3.5 Butt-welded joints in VPPA-GMAW process

Butt-welded joints are achieved by VPPA-GMAW process on 7A52 aluminum alloys with thickness of 10 mm. The optimized welding parameters are as follows: DCEN current of 130 A, DCEP current of 182 A, the ratio of DCEN to DCEP time of 20 ms : 4 ms, GMAW current of 320 A, orifice gas flow rate of 3.5 L·min^{-1}, MIG shielding gas flow rate of 23 L·min^{-1}, overall shielding gas flow rate of 40 L·min^{-1}, welding speed of 420 mm·min^{-1}, and the distance of 10 mm from nozzle to workpiece. Weld joint design is square groove joints welded from one side with backing, and the morphology of weld seam is shown in Fig. 9. There are no undercut and hump defect on weld seam. Meanwhile, clear fish scale can be observed on front side of weld seam, and back side of weld seam surface is smooth and uniform.

4 Conclusion

In VPPA-GMAW process, it is quite easy for the droplet to fall off the wire when the electromagnetic force gradually increases during pulse period. During base period, droplet movement through the arc zone is further accelerated since

the central pressure of arc column increased. There is significant difference in droplet speed arriving at the pool between VPPA-GMAW and GMAW processes. The droplet momentum in VPPA-GMAW process is larger than that in conventional GMAW process. And the former increases with increasing plasma current in a certain range, thus being appropriate for welding thick-plate aluminum alloys. Butt welds are achieved by VPPA-GMAW process on 7A52 aluminum alloys with thickness of 10 mm. Clear fish scale can be observed on front side of weld seam, and weld seam surface on back side is smooth and uniform.

Acknowledgments This research effort was supported by the National Science Foundation of China (Grant Number: 51365032).

References

1. Thomsen JS (2006) Control of pulsed gas metal arc welding. Int J Model Identif Control 1(2):115–125
2. Wang XW, Huang Y, Zhang YM (2013) Droplet transfer model for laser-enhanced GMAW. Int J Adv Manuf Technol 64(1-4):207–217
3. Mao YQ, Ke LM, Liu FC, Huang CP, Chen YH, Liu Q (2015) Effect of welding parameters on microstructure and mechanical properties of friction stir welded joints of 2060 aluminum lithium alloy. Int J Adv Manuf Technol 81(5-8):1419–1431
4. Balasubramanian V, Ravisankar V, Reddy GM (2008) Effect of pulsed current welding on mechanical properties of high strength aluminum alloy. Int J Adv Manuf Technol 36(3-4):254–262
5. Essers WG, Liefkens AC (1972) Plasma-MIG welding developed by Philips. Mach Prod Eng 1(11):632–633
6. Ono K, Liu ZJ, Era T, Uezono T, Ueyama T, Tanaka M, Nakata K (2009) Development of a plasma MIG welding system for aluminium. Weld Int 23(11):805–809
7. Sevim I, Hayat F, Kaya Y, Kahraman N, Sahin S (2013) The study of MIG weldability of heat-treated aluminum alloys. Int J Adv Manuf Technol 66(9-12):1825–1834
8. Yang T, Gao HM, Zhang SH, Wu L (2013) Interface behavior of copper and steel by plasma-MIG hybrid arc welding. Acta Metall Sin (Engl Lett) 26(3):328–332
9. Hertel M, Fussel U, Schnick M (2014) Numerical simulation of the plasma-MIG process–interactions of the arcs, droplet detachment and weld pool formation. Weld World 58(1):85–92
10. Bai Y, Gao HM, Lu H, Shi L (2006) Analysis of plasma-MIG arc signal based on LABVIEW. Trans China Weld Inst 27(8):59–62
11. Bai Y, Gao HM, Qiu L (2010) Droplet transition for plasma-MIG welding on aluminium alloys. Trans Nonferrous Met Soc China 20(12):2234–2239
12. Ton H (1975) Physical properties of the plasma-MIG welding arc. J Phys D: Appl Phys 8(8):922–933
13. Terasaki H, Simpson SW (2005) Modelling of the GMAW system in free flight and short circuiting transfer. Sci Technol Weld Joining 10(1):120–124
14. Essers WG, Walter R (1981) Heat transfer and penetration mechanisms with GMA and plasma-GMA welding. Weld J 60(2):37–42
15. Resende AA, Ferraresi VA, Scotti A, Dutra JC (2011) Influence of welding current in plasma-MIG weld process on the bead weld geometry and wire fusion rate. Weld Int 25(12):910–916
16. Chen SJ, Jiang F, Zhang JL, Huang N, Zhang YM (2013) Principle of weld formation in variable polarity keyhole plasma arc transverse welding of aluminum alloy. Trans China Weld Inst 34(4):1–6
17. Zhang QL, Fan CL, Lin SB, Yang CL (2014) Novel soft variable polarity plasma arc and its influence on keyhole in horizontal welding of aluminium alloys. Sci Technol Weld Joining 19(6):493–499
18. Woodward NJ, Richardson IM, Thomas A (2000) Variable polarity plasma arc welding of 6.35 mm aluminium alloys: parameter development and preliminary analysis. Sci Technol Weld Joining 5(1):21–25
19. Han YQ, Zhao P, Du MH, Yao QH (2012) Numerical simulation of aluminum alloys variable polarity plasma arc welding temperature field. Chin J Mech Eng 48(24):33–37
20. Han YQ, Hong HT, Guo L, Yao QH (2013) Vertical welding of aluminum alloy during variable polarity plasma arc welding process with AC-DC mixing output current. Trans China Weld Inst 34(9):59–62
21. Zhang W, Hua XM, Liao W, Li F, Wang M (2014) Behavior of the plasma characteristic and droplet transfer in CO_2 laser-GMAW-P hybrid welding. Int J Adv Manuf Technol 72(5–8):935–942
22. Scotti A, Rodrigues CEAL (2009) Determination of momentum as a mean of quantifying the mechanical energy delivered by droplets during MIG/MAG welding. Eur Phys J Appl Phys 45(1):1–8
23. Waszink JH, Piena MJ (1986) Experimental investigation of drop detachment and drop velocity in GMAW. Weld J 65(11):289–298
24. Reis RP, Souza D, Scotti A (2011) Models to describe plasma jet, arc trajectory and arc blow formation in arc welding. Weld World 55(3–4):24–32
25. Lancaster JF (1986) The physics of welding. Pergamon Press, Oxford